Concrete Evaluation by Radar Theoretical Analysis

A.V. ALONGI, T.R. CANTOR, C.P. KNEETER, AND A. ALONGI, JR.

The operating principles of a mobile high-resolution radar system that has been optimized for inspection of pavements such as highways, bridge decks, and runways are described. The waveforms generated by the high-resolution radar are illustrated as well as the interaction of these waveforms with the pavement structure. Graphic derivations of representative radar waveforms for varying conditions are shown by using time-domain analysis. This simplified method of analysis enables useful models to be made for a range of separation thicknesses and pavement base materials. The results of laboratory tests are presented in which radar illuminates a double slab of concrete and the spacing between the two slabs is varied discretely and precisely from 0 to 30 cm (0 to 12 in). For spaces up to 7.5 cm (3 in) between two similar materials, the amplitude of the radar echo appears to be nearly proportional to the same dimension. As the space increases to 15 cm (6 in), the signal increases primarily in width. For spaces greater than 15 cm, the radar signal splits into two separate waveforms, thereby resolving the upper and lower boundaries of the space. These laboratory data are related to in situ void data taken on airport runways. Finally, a detailed analysis of a single concrete slab, illuminated by the radar, is performed. The amplitude and phase properties of the reflected signal waveforms are derived independently based on time-delay measurement and a mathematical method. Both methods agree with each other and with the experimental data.

As soon as a concrete structure in the infrastructure is poured, aging and accompanying deterioration start. The earlier the regression or impending fault can be discovered by nondestructive techniques, the easier and less costly it is to correct and the better is the chance of reducing user inconvenience. Such a system of maintenance is highly desirable.

Early in the 1970s, it was realized that radar, developed in the 1960s under contract with the U.S. Army to detect nonmetallic mines, might be modified for concrete evaluation and void detection. In its currently modified form, it is referred to as concrete inspection radar (CIR).

This paper deals with the theoretical concepts that form the basis for currently successful operation of CIR. An analysis is made of the synthesization of the received wave shape as well as a determination of the energy levels reflected at the various interfaces, such as air and concrete or concrete and base material. In addition, determination of space signals between two 15-cm (6-in) concrete blocks is demonstrated.

It should be noted that the word "voids" is used in this paper for illustrative purposes, and in the case of concrete it generally refers to small separations, cracks, or microcracks that determine the condition or serviceability of concrete.

OPERATING PRINCIPLES OF HIGH-RESOLUTION RADAR

Materials either man-made or occurring in nature are conveniently classified as metal or dielectric from an electromagnetic viewpoint. Metallic substances are generally good conductors, both electrical and thermal, whereas dielectric substances are poor conductors. Radio frequency (RF) waves are capable of penetrating and propagating through dielectric materials and tend to be almost totally reflected from metallic materials. Thus, an RF wave from a radar transmitter at an airport, for example, propagates through a dielectric medium, the air in this case, strikes a metallic boundary such as the skin of the aircraft, and is reflected back to the radar receiver; the aircraft angle and distance can then be identified. Similarly, an electromagnetic radio wave emitted by high-resolution radar into a dielectric material such as a pavement structure will propagate through the material until it intercepts a boundary. A boundary is any discontinuity or differing dielectric, such as air to asphalt, asphalt to concrete, change in concrete, and fractures and separations. At the boundary, a portion of the incident energy will be reflected and a portion will be transmitted through the boundary. These phenomena are governed by well-established physical laws, as illustrated later in this paper. Field application of the principle is discussed in the paper by Cantor and Kneeter elsewhere in this Record.

RADAR WAVEFORMS

A brief explanation of the waveforms generated and transmitted by high-resolution radar will assist in understanding the results and analysis of the interaction of the radar waveform with materials. The radar generates a repetitive pulse, of which a single radar cycle waveform is shown in Figure 1 (waveform 1a). The signal is radiated by the antenna into air and, when received, the return signal looks like waveform 1b. If the radiated waveform happens to intercept a boundary, such as air to concrete or air to metal, the reflected waveform that is received looks generally like waveform 1c. Boundaries between different materials have different reflection coefficients (1), from 0.2 for sand to 1.0 for metal, thus giving different amplitudes for the return echo. The reflection coefficient (ρ) determines the amount of energy returned from the material surface, top, bottom, or internal. The amplitude of the surface echo is indicative of its reflection coefficient, which allows classification of the surface material--i.e., concrete or blacktop. Waveform 1d in Figure 1 is more representative of the actual surface echo when the antenna is 20 cm (8 in) from the surface, the preferred operating distance. The pulling down of the first negative peak is caused by antenna end effect, and the true surface echo or return is measured from the large positive peak and the second negative peak (first negative peak after positive peak).

Subsequent echoes arising from boundaries within the pavement are further separated in time from the antenna end effect, and the shapes of their echoes are not affected by it. Note that measurements made in the laboratory are more susceptible to "multiple time around effects"--i.e., internal "re"-reflections (see waveform 2c in Figure 2)--because the samples under test are not terminated with an infinite thickness of base material, which greatly reduces the multiple time around effect. This can be noted in the laboratory test data but does not affect the analysis or interpretation of the data, since it is later in time and can be ignored or considered as noise.

GRAPHIC DERIVATION BY TIME-DOMAIN ANALYSIS

One of the chief advantages of a high-resolution radar is that it generates a very short pulse in time, approximately 1 ns (10^{-9} s), thereby allowing maximum resolution of boundaries or objects. Although one-half of a pulse width, or 15 cm (6 in) in air and approximately 5.5 cm (2.2 in) in asphalt or concrete, is an apparent theoretical limit of resolution, by taking advantage of the algebraically summed overlapped and time-displaced signal, it is possible to resolve distances down to crack widths.

Figure 1. Radar waveforms.

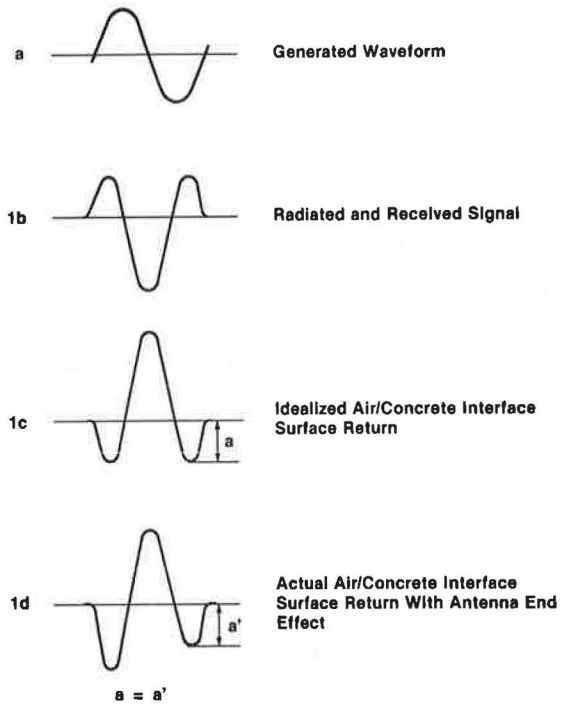

Figure 2. Graphic separation analysis.

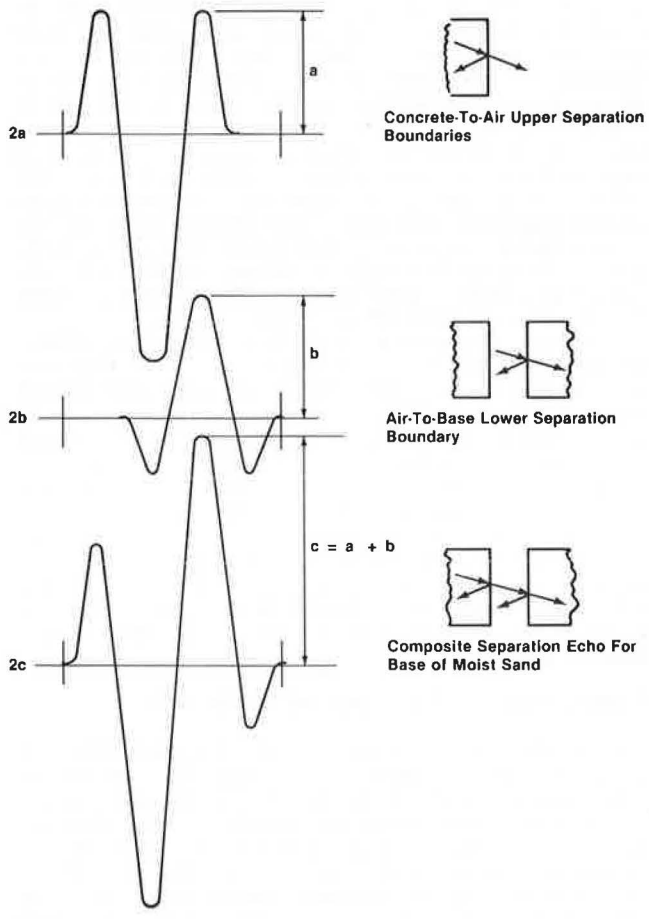

The amplitudes of the signal of the upper and lower void boundaries are derived by means of the reflection and transmission coefficients related to the dielectric materials encountered. In the analysis, it is assumed that the materials are "lossless", homogeneous, and frequency independent for the frequency spectrum of the transmitted waveform. This method can easily accommodate "lossy" materials by adjusting the transmission coefficient for the ray through the slab to include a loss factor. One other assumption is made--that the relative permeability is unity, which is the case for almost all pavement materials.

As an example, for an air space, a typical composite echo can be synthesized from two radar echoes that are less than half a pulse width apart. Given the waveforms shown in Figure 1, and by applying the principles of reflection and transmission of electromagnetic waves when they interact with dielectric substances, one can perform direct time-domain analyses that yield excellent results and correlate well with laboratory and field tests on voids (2). This simplified method of analysis is helpful in understanding the separation echo waveshape as a function of thickness and the dielectric properties of the space boundary. Thickness of void is constant at 6.25 cm (2.5 in).

In Figure 2, waveform 2a is the radar waveshape from the top of a concrete-to-air separation. For the separation chosen, 6.25 cm or about one-third of the radar pulse width, the isolated echo from the bottom boundary of the separation would be as shown in waveform 2b. Note the time displacement phase shift to waveform 2b with respect to waveform 2a. The algebraic sum of the two waveforms is as shown in waveform 2c. This resultant separation waveshape has the following properties: It is larger in amplitude than the other two; its width extends from the beginning of waveshape 2a to the end of waveshape 2b; it has a strong negative peak followed by a strong positive peak. These characteristics are almost always found in a separation echo. Waveform 2a is thus the echo of an infinite separation; that is, there is no bottom boundary echo to sum with it. Waveform 2b represents the reflection from the bottom boundary of the separation whose base material is slightly moist sand.

In Figure 3, waveform 3a shows the graphically derived composite separation echo for a totally dry sand base. This represents a limiting case since, in situ, the base would always have some moisture content. Observe that the composite echo is slightly smaller, peak to peak, than the previous echo in waveform 2c. However, the waveshape is still similar--negative and then positive major peaks; the first small positive peak is larger than the last small negative, and the complete echo waveform still has the same width.

Waveform 3b in Figure 3 is for two concrete slabs. This represents a pavement delamination if the separation is allowed to become very small. As the void approaches 0 cm, the echo from the upper and lower boundaries would cancel out because of phase relationship and spacing. Note that the peak-to-peak amplitude of waveform 3b is larger than that of waveforms 2c and 3a because the bottom reflection is stronger. The waveshape is first negative going, in its major peak, and this is then followed by a positive going major peak. The small leading and trailing positive and negative waveform components are almost equal. This case may also be representative of separations (voids) beneath pavements when the base material is crushed stone and sand.

If the bottom boundary of the separation is water saturated, or water, then the composite waveform would be like waveform 3c. The peak-to-peak ampli-

tude is much greater, about 1.5 times that of dry sand. However, the pulse width is still the same since it is determined solely by the separation distance. Note that the small negative trailing waveform is now larger than the small positive leading waveform; the major waveform peaks are still first negative and then positive, characteristic of separations.

Figure 3. Graphic separation analysis: base material variation.

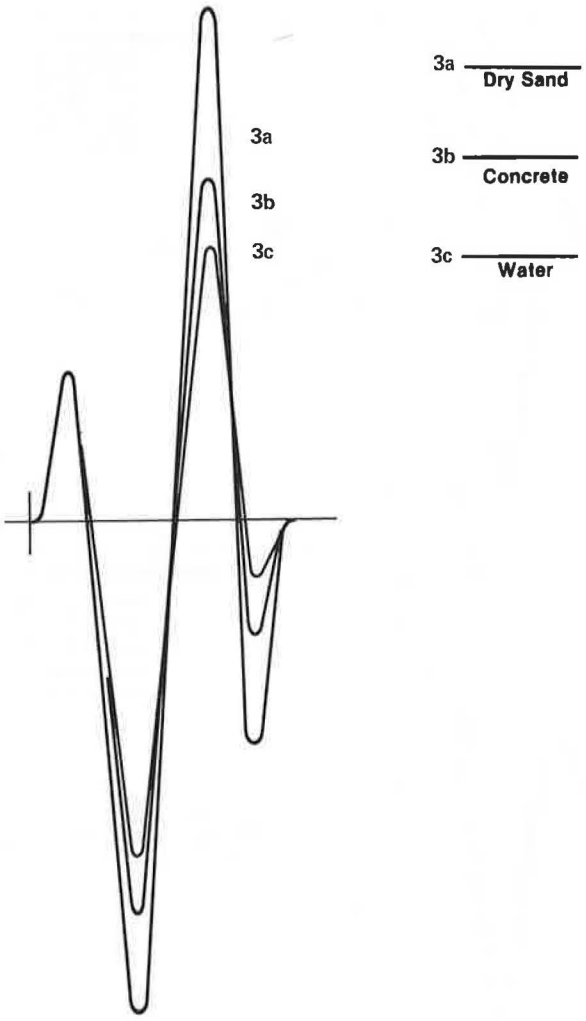

Although this technique has been illustrated for a single separation, it can be used directly for other distances by changing the time displacement between the top and bottom echoes.

For a given pavement thickness, when no separation is present beneath it, an estimate can be made of the material property of the base. The radar data show the time delay between the surface and the boundary echoes. They also show the ratio of the surface to boundary echo amplitudes that permits this determination.

SIGNAL MODIFICATION BY SPATIAL CHANGE

Two 0.9-m-square (3-ft-square) concrete slabs, both 15 cm (6 in) thick, were moved from 0 to 30 cm (0-12 in) apart, one behind the other, and the radar antenna was positioned perpendicular to the 0.9-m (3-ft) face. The radar return waveforms are shown for the various distances in Figures 4-7.

In Figure 4, the radar separation echoes are shown superimposed for 0-, 6-, 12-, 18-, and 25-mm (0-, 0.25-, 0.5-, 0.75-, and 1-in) spacings. These waveforms have features identical to those of the graphically derived waveforms 2c through 3b shown earlier in Figures 2 and 3, especially waveform 3b, since it was derived for two concrete slabs. The echoes all start at the same point in time. There is a leading edge minor peak followed by the leading major negative peak, the characteristic of a void, and this is then followed by a major positive peak and then by a trailing minor negative peak. As the separation is increased, the pulse width is increased, as shown by the slope in the positive and negative peaks.

Figure 5 very clearly shows the point in time at which the composite separation echoes start and the point at which the internal "re"-reflections occur. Figure 6 shows the difference in ending for the various echoes from 75 to 175 mm (3-7 in) and broadening of the waveform. Figure 7 shows the splitting of the waveform at 200-mm (8-in) separation, which resolves the boundary closest to the antenna from the boundary farthest from the antenna. In Figure 8, the echo waveform further splits as the separation goes from 250 mm to 300 mm (10-12 in).

The data demonstrate signal change as the separation increases. The first echoes arising from the bottom of the first 15-cm (6-in) block are all in phase due to the fixed thickness of the slab. The echoes from the bottom boundary, the top of the

Figure 4. Radar separation echoes for two 15-cm blocks: 0- to 25-mm air separation.

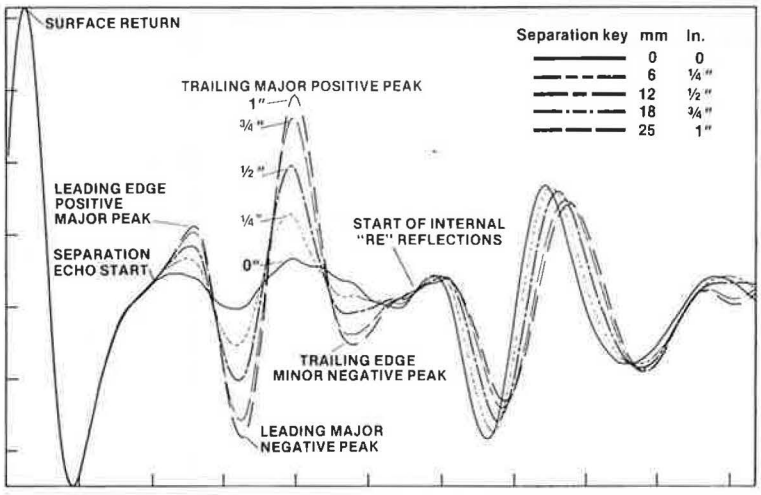

second 15-cm (6-in) block, discretely define the 2.5-cm (1-in) displacements for the 25-, 27.5-, and 30-cm (10-, 11-, and 12-in) spacing between slabs. The "two time around" or internal "re"-reflections of the first echo in the block closest to the radar interfere with the echo from the bottom boundary, which produces a characteristic effect. For an alternative presentation of these data, see the paper by Cantor and Kneeter elsewhere in this Record.

The data shown in Figure 9 were taken at an airport runway and are shown to illustrate the manner in which the laboratory knowledge was carried into field investigations. The two correlated well. Observe the spacing waveforms increasing with depth, which indicates an increasing separation, as was found in the field.

An inspection was made by means of high-resolution radar to determine the location of suspected

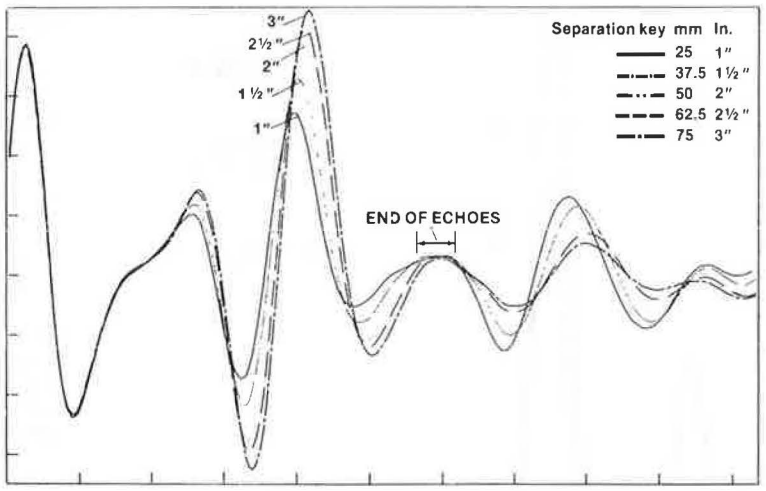

Figure 5. Radar separation echoes for two 15-cm blocks: 25- to 75-mm air separation.

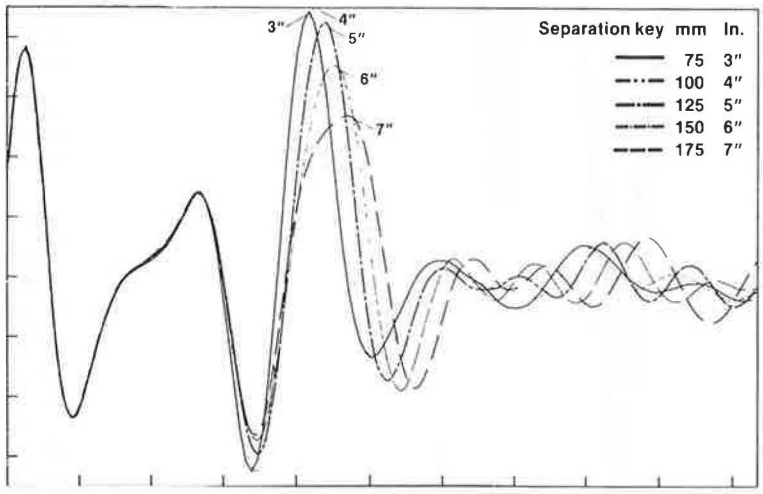

Figure 6. Radar separation echoes for two 15-cm blocks: 75- to 175-mm air separation.

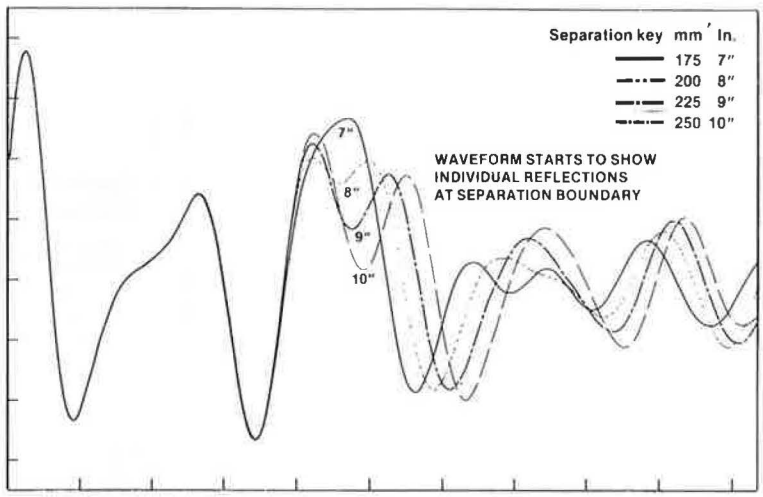

Figure 7. Radar separation echoes for two 15-cm blocks: 175- to 250-mm air separation.

Figure 8. Radar separation echoes for two 15-cm blocks: 250- to 300-mm air separation.

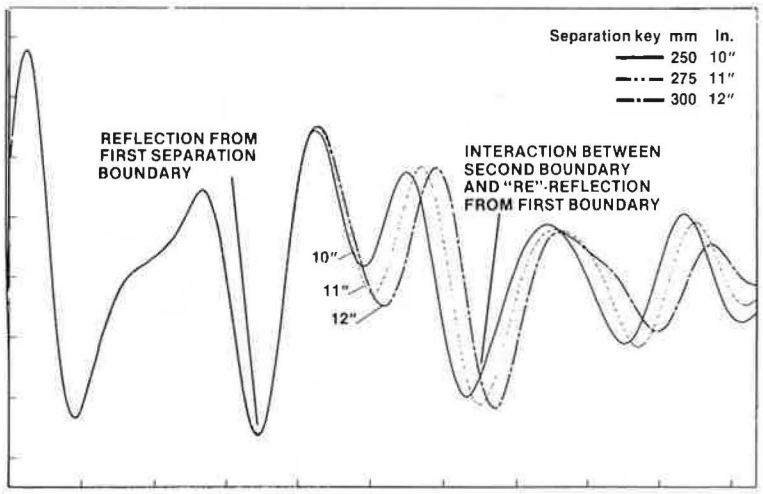

Figure 9. Void under runway.

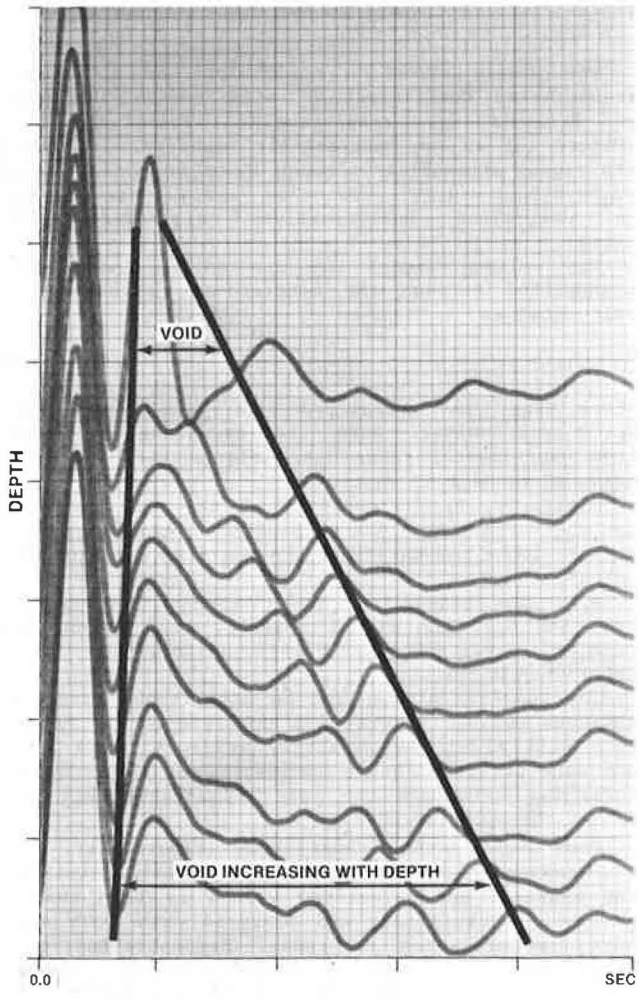

Figure 10. Ray diagram.

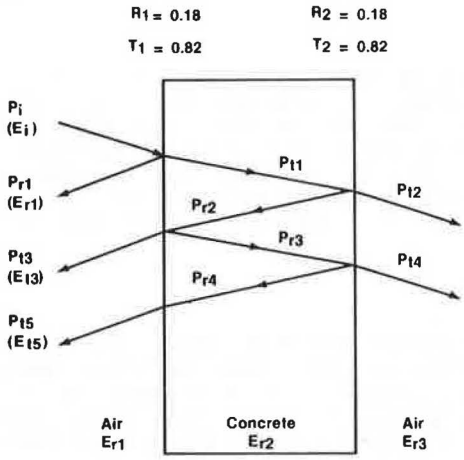

voids. Test borings made at the radar-indicated locations provided positive confirmation. The voids varied in thickness from 3 to 75 mm (0.125-3 in) although, as just reviewed, larger voids can be accommodated (3).

MATHEMATICAL ANALYSIS OF RADAR WAVES

The previously presented experimental data have been evaluated by analytical inductive and deductive methods. Quantitative methods are frequently helpful in explaining and corroborating this type of information. Therefore, a simplified mathematical method for analyzing radar data is discussed here that provides a data base for understanding and transferring knowledge for interpreting various waveforms.

The following assumptions and approximations are made: (a) All surface boundaries are in the plane perpendicular to the radar antenna, and (b) all dielectric materials are considered uniform, homogeneous, and frequency independent.

Figure 10 shows a ray diagram that depicts the transmissions through and reflections from the boundaries of different dielectric materials, air to concrete and concrete to air. Epsilon (ε) is the dielectric constant for the material and determines the time of travel of the electromagnetic wave through the medium, i.e., permittivity. Air has a known dielectric constant (ε_r) of approximately unity, and concrete has a calculated dielectric constant (ε_{r2}) of 6.11 (4). The voltage reflection coefficient (ρ) at the air-to-concrete boundary has also been calculated to be -0.424.

The power of the incident electromagnetic wave must be known to determine boundary reflection magnitude. The incident power, determined experimentally and normalized with respect to free-space (air) impedance, yielded a value of 33.06 units^2.

Figure 11. Experimental verification.

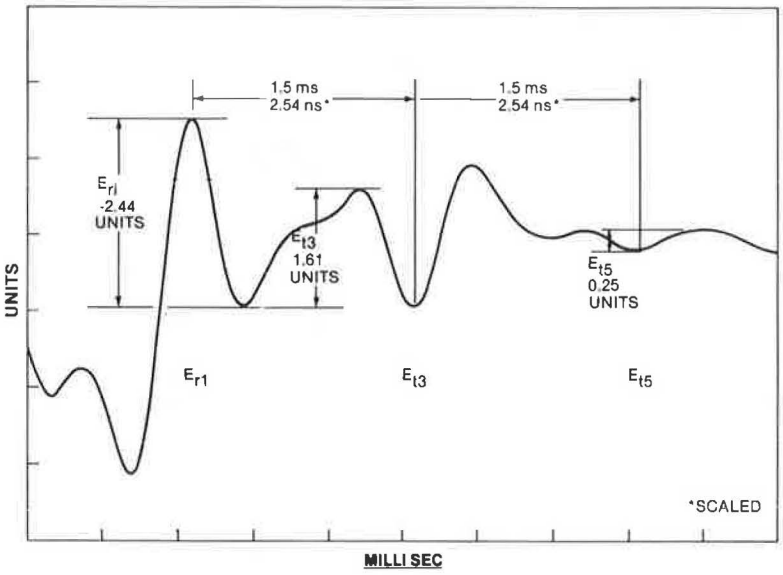

Ideally, the power transmitted (P_i) into a dielectric boundary or interface must equal the power reflected from the boundary (P_r) plus the power transmitted through the boundary (P_t)--i.e., $P_i = P_r + P_t$. At the air-concrete interface shown in Figure 9, the power reflected (P_r) can be solved if R, the power reflection coefficient, is known.

$$R_{n,n+1} = (\rho n, n+1)^2 \quad (1)$$

where n is the current medium and n+1 is the medium to be next penetrated. The voltage reflection coefficient ($\rho_{air/concrete}$) was calculated to be -0.424. $R_{air/concrete} = 0.18$. For this, the power transmission coefficient (T) can be determined:

$$T_{n,n+1} = 1 - R_{n,n+1} \quad (2)$$

$T_{air/concrete} = 0.82$.

The power P_{r1} reflected at the air-concrete boundary (Figure 9) can now be calculated: $P_{ri} = R_1 P_i = 5.95$ units^2.

The voltage signal E_{r1} due to the power P_{r1} reflected is determined to be and is calculated as

$$E_{r1} = (P_{r1})^{1/2} \quad (3)$$

where P_{r1} is normalized with respect to air impedance. The negative sign corresponds to a voltage polarity inversion. Thus, $E_{r1} = -2.44$ units. From experimental data (Figure 2), E_{r1} was measured at -2.44 units.

The magnitude of P_{t1}, transmitted power, can be calculated from the relation, $P_{t1} = T_1 P_i = 27.11$ units^2.

The signal attenuation for this concrete was calculated to be -0.154 dB/in of concrete from the flat plate experiment. Therefore, 15 cm (6 in) of concrete attenuation (A) is -0.924 dB for a power ratio of 0.806 and a signal decrease of about 20 percent. P_{t1} (Figure 10), at the concrete-air boundary, after traversing 15 cm of concrete, will then be $P_{t1} = T_1 P_i A = 21.85$ units^2.

Next, calculate P_{r2}, the power reflected back from the concrete-air boundary. It can be shown that the voltage reflection coefficient at the concrete-air interface will be the negative of that at the air-concrete interface: $\rho n, n+1 = -\rho n+1, n$.

The power reflection coefficient R_2 and power transmission coefficient T_2 will remain the same as R_1 and T_1, respectively. Therefore, P_{r2} (Figure 10) at the concrete-air boundary, including the signal attenuation through 15 cm of concrete, is $P_{r2} = R_2 P_{t1} A = 3.17$ units^2. P_{t3} can now be determined analytically: $P_{t3} = T_1 P_{r2} = 2.6$ units^2.

The voltage signal E_{t3} due to the power P_{t3} transmitted through the concrete-air interface is calculated as

$$E_{t3} = (P_{t3})^{1/2} \quad (4)$$

where P_{t3} is normalized for air impedance: $E_{t3} = 1.61$ units. Note the excellent agreement from experimental radar data (Figure 11): E_{t3} was measured to be 1.63 units.

Similarly, P_{r3} (Figure 10) at the back boundary is $P_{r3} = P_{r2} \cdot R_1 \cdot A = 0.46$ units^2. Likewise, P_{r4} at the front boundary is $P_{r4} = P_{r3} \cdot R_2 \cdot A = 0.0667$ units^2.

P_{t5}, the transmitted power through the boundary, and E_{t5}, the signal voltage, can now be determined: $P_{t5} = P_{r4} T_1 = 0.0547$ units^2, and $E_{t5} = (P_{t5})^{1/2} = 0.234$.

The polarity of E_{t5} can be established since an incident voltage wave from a concrete-to-air interface will always be partially reflected back with the same polarity as the incident wave (5). Therefore, E_{t5} will have the same polarity as E_{t3} and E_i but the opposite of E_{r1}.

From experimental radar data (Figure 11), E_{t5} was measured to be 0.25 unit. The deviation between the measured and calculated values is less than 6 percent. Thus, theory and measured data both support the abilities of radar, demonstrating that radar data can be analyzed through simplified mathematical means with results that closely agree with the experimental. Although we have taken a simplified example for illustrative purposes, the method of data analysis outlined here can be extended to a variety of more complicated cases.

CONCLUSIONS AND RECOMMENDATIONS

Based on data developed in this paper, which consist of examination of waveforms, graphic evaluations, mathematical analysis, and laboratory and field

experiments, it can be concluded that CIR is an appropriate technology for evaluating the condition of concrete up to 75 cm (30 in) in depth by differentiating between serviceable concrete and deteriorated concrete, which consists of delaminations, deteriorations, microcracks, and cracks up to and including small voids. This is further supported by the field experiences described in the paper by Cantor and Kneeter elsewhere in this Record.

The following recommendations are made:

1. Theoretical analyses followed by field tests have successfully demonstrated the ability of radar to detect changes in materials and locate where these changes occur. It is therefore recommended that the system be enhanced for field operations.
2. It is further recommended, as considered in the paper by Cantor and Kneeter in this Record, that the CIR be made completely automatic, including signal processing and data handling, so that the radar system can be used as a maintenance management tool to provide greater cost benefit for roadway repair with minimum inconvenience to the riding public.

ACKNOWLEDGMENT

The contents of this paper reflect our views and do not necessarily reflect the views of Penetrader Corporation or the Port Authority of New York and New Jersey.

REFERENCES

1. A.R. Von Hippel. Dielectrics and Waves. M.I.T. Press, Boston, MA, 1966.
2. J.A. Stratton. Electro-Magnetic Theory. McGraw-Hill, New York, 1941.
3. A. Alongi. Model PS-24 Penetradar and Technical Notes PTN-001 and 002. Penetradar Corp., Niagara Falls, NY, 1981.
4. A.G. Kandoian and others. Reference Data for Radio Engineers, 4th ed. International Telephone and Telegraph, New York, 1956.
5. L.F. Woodruff. Electric Power Transmission. Wiley, New York, 1946.

Publication of this paper sponsored by Committee on Performance of Concrete.

Radar as Applied to Evaluation of Bridge Decks

T.R. CANTOR AND C.P. KNEETER

Approximately 90 percent reliability has been achieved in nondestructively identifying good and deteriorated concrete on a bridge deck, based on experimental research in the laboratory and field. The ability of concrete inspection radar to function reliably and repeatably in identifying the condition of concrete is established. Ability to detect voids is commented on. Present signal processing, data analysis, and interpretation via cluster analysis constitute a lengthy manual operation. However, with computer-assisted data automation, the system should be a viable field instrument operable by a technician.

Concrete inspection radar (CIR) has demonstrated its capability to reliably perform in the field as a nondestructive evaluation (NDE) tool for determining the condition of concrete (1-3). CIR has identified good and distressed concrete with 90 percent confidence (4).

Physical laboratory studies performed to calibrate the equipment and understand physical parameters include detection of voids, effects of steel, multiple material layers, antenna direction and angularity, water, temperature, and edge (5).

Included in the laboratory analytical studies were various signal-processing techniques, among which were topographic displays, photographic superimposition, graphic signature identification techniques, and mathematical models (3). Of the mathematical models, cluster analysis has resulted in the most reliable and least time-consuming classification of concrete (6).

The field operations were conducted on several major structures. Among the factors studied were reproducibility, influence of reinforcing steel, and varying void depths. The field investigation culminated in the physical verification of the concrete condition as interpreted by the analysis of the radar data (4).

To verify the radar-predicted conditions of distressed and good concrete, a physical evaluation was undertaken by field drilling. Depth of drilling was ranked and statistically analyzed and led to a physically verified confidence of 90 percent (4).

Automation of the present manual data processing by direct computer operation will make CIR a field system operable by a technician and capable of identifying and differentiating good and distressed concrete.

INTRODUCTION TO CIR

Starting at pouring of concrete, every structure in the infrastructure begins to deteriorate with time. The first evidence of this, generally, is surface cracking. With roads, riding surfaces may hide these defects until, in many cases, serious problems exist. Once water enters the cracks, deterioration increases more rapidly, because of either freeze-thaw stresses or rebar corrosion. The earlier the fault or impending fault can be detected, the less costly and easier it is to repair, with minimum inconvenience to the users of the facility (7).

The search to obtain an NDE tool capable of detecting deterioration as early as possible led Port Authority of New York and New Jersey (PANYNJ) Engineering Research and Development engineers down many paths, the most successful of which has been CIR (8).

Interest in radar as a possible NDE tool stemmed from radar development work by Calspan Corporation (9) in the mid-1960s, under U.S. Army contract, to detect buried nonmetallic mines. Subsequent CIR modifications allowed it to be used in the early 1970s to detect voids under pavements (1,2). Follow-up studies of this radar development work by PANYNJ Engineering Research and Development staff in 1974 led to the program of radar NDE testing and development described in this paper (10).